Mechanisms by Which Pulsatile Flow Affects Cross-Flow Microfiltration

Hong-yu Li and Christopher D. Bertram
Graduate School of Biomedical Engineering, The University of New South Wales, Sydney, Australia 2052

Dianne E. Wiley
UNESCO Centre for Membrane Science and Technology, The University of New South Wales, Sydney, Australia 2052

The effect of pulsatile flow on particle deposition during cross-flow microfiltration was studied to establish the degree to which backflushing and shear-rate changes induced during pulsation alter cake formation. The minimum transmembrane pressure and maximum absolute cross-flow velocity derivative were chosen to quantify the backflushing and shear effects, respectively. Experiments were conducted for pulsatile flows with four distinct types of transmembrane pressure and flow-rate waveforms. In the absence of backflushing, the cake resistance was reduced at high values of shear rate, but not significantly affected at low values compared with steady flow. Tests at constant shear rate demonstrated that the cake resistance was reduced when backflushing was imposed on the system. In tests with two transmembrane pressure waveforms, cake deposition was almost completely eliminated by instantaneous backflushing. Although both backflushing and shear-rate changes reduce cake deposition in microfiltration, backflushing achieved the greatest reductions.

Introduction

Cross-flow microfiltration has grown to be a mature industrial process in the past 30 years. Many inexpensive techniques have been developed to reduce the decline in flux usually observed during cross-flow microfiltration. Several review papers (Ilias and Govind, 1990; Spiazzi et al., 1993; Winzeler and Belfort, 1993) have summarized strategies for controlling flux decline. Depending on the factors causing flux decline in specific applications, the control can be placed in one of three categories: modification of membrane, modification of feed, and modification of fluid dynamics in the membrane module. Among these approaches, modification of the fluid dynamics has been the most popular.

Inducing pulsatile flow in membrane modules is one of the most promising techniques for modifying the fluid dynamics. Many successful examples have been reported over the last ten years (Bertram et al., 1993; Ding et al., 1991, 1993; Gupta et al., 1986, 1992; Jaffrin, 1989; Jaffrin et al., 1987, 1989, 1992, 1994; Rodgers and Sparks, 1991, 1992; Wenten et al., 1994). Among the mechanisms proposed to explain enhanced performance in microfiltration, Ding et al. (1993), Gupta et al. (1986), and Jaffrin et al. (1994) suggested that pulsation produced enhanced shear when flow reversal of the bulk solution was achieved. Spiazzi et al. (1993) suggested that the flux was affected by the maximum of the cross-flow velocity.

In a detailed comparison of the filtrate flux and pressure waveforms and pressure wave, Gupta et al. (1992) reported that flux enhancement with a pressure wave involving a short-duration (relative to cycle length) minimum followed by a short-duration maximum was higher than when the maximum preceded the minimum. They postulated that, after a stable pressure period during which a cake was formed, a low-pressure peak caused destabilization of the cake layer. Then during the high-pressure peak, high shear removed many particles from the cake layer. With a waveform in which the high-pressure peak followed the stable pressure period, the high maximum shear removed fewer particles from the cake layer than when the boundary layer was destabilized first.

Rodgers and Sparks (1991, 1992) reported that transmembrane pressure pulsing was more effective than the shear rate

Correspondence concerning this article should be addressed to Hong-yu Li.

in increasing permeate flux. They showed that pulsing of the permeate prevented the development of a cake on the membrane surface, thereby reducing filtration resistance and increasing flux. They attributed the effect of the pulsatile flow on the flux enhancement to a translation of body force through the membrane altering the concentration polarization boundary layer. A similar "backshock process" was applied by Wenten et al. (1994) to the filtration of yeast.

A previous report from this laboratory (Bertram et al., 1993) presented the experimental investigation of collapsible-tube-generated pulsatile-flow cross-flow microfiltration. That study demonstrated that the collapsible-tube-generated pulsatile flow was efficacious in the cross-flow microfiltration process over a wide range of operating conditions of cross-flow velocity, transmembrane pressure, and solids concentration. In addition, analysis of the pulsatile parameters provided the following insights into the relationship between flux enhancement and pulsatile parameters: (1) the ratio of the cake resistance in pulsatile flow to that in steady flow was more strongly correlated with pressure-related variables than with flow-related variables, and (2) the cake resistance ratio was most strongly correlated with the minimum pressure.

This article presents a further study on the effect of pulsatile flow on particle deposition in the cross-flow microfiltration. This study has demonstrated that it is possible, by suitable choice of pulsatile conditions, essentially to eliminate the formation of cake during cross-flow microfiltration. The cake resistance can be reduced at high values of shear-rate-related parameters, as well as when backflushing is imposed on the system, compared with steady flow. Although both backflushing and shear-rate changes can be utilized to reduce cake deposition in microfiltration, backflushing achieves the greatest reductions.

Proposed Mechanisms

Backflushing mechanism

In our previous work (Bertram et al., 1993) we found a direct correlation between cake reduction and increasing negative values of minimum transmembrane pressure $P_{\min}$. We reasoned that during the period of negative transmembrane pressure, the transmembrane flow was from the permeate side to the feed side. This back flow of the permeate then carried the particles deposited on or near the membrane surface back to the bulk feed flow. In this way the cake on the membrane surface was eliminated or reduced.

To examine the effect of backflushing on cake reduction, the transmembrane pressure waveform, which indicates both the duration and the magnitude of the negative pressure, can be parameterized. In this article, we have again chosen the minimum value of the instantaneous transmembrane pressure, $P_{tm}(t)$, to quantify the extent of backflushing.

Shear-related mechanism

For techniques involving pulsatile flow without a negative pressure peak, various researchers (Jaffrin, 1989; Jaffrin et al., 1987, 1989, 1992, 1994; Kennedy et al., 1974) have reported that the filtration performance was still improved over that obtained for steady flow. These researchers have suggested that, in pulsatile flow, the shear rate near the membrane wall was increased. According to the well-known shear-induced diffusion model (Davis and Birdsell, 1987; Zydney and Colton, 1986) or scour model (Fane, 1986), it is assumed that more particles are carried back to the bulk flow by higher shear.

To examine the effect of shear, the shear waveform at the membrane surface should be measured and the mean, root mean square (rms), or maximum wall shear evaluated. However, the temporal maximum in the shear is probably the main factor responsible for flux improvement. Since the shear scouring effect is not direction-dependent, the maximum of the absolute value of shear can be used.

In our experiments we did not measure shear directly, but determined it indirectly by measurements of flow-rate and pressure as follows. It must also be noted that the crossflows were turbulent in our microfiltration system (Li, 1995). Thus shear at the membrane wall could not be estimated directly from theoretical equations. Studies of velocity profiles for laminar pulsatile flows at high Womersley numbers [$\alpha \equiv r(\omega/\nu)^{1/2} \gg 1$] in straight tubes show that the greatest velocity gradients occur in the fluid layer near the wall (McDonald, 1974). Therefore studies of fluid dynamics in the Stokes layer have been adapted to provide insights into how the shear near the wall can be related to other measurable parameters.

Batchelor (1970) showed that pressure is approximately uniform across the boundary layer. Therefore the pressure gradient along the boundary layer is the same as the pressure gradient of the bulk solution in the axial direction, approximated in this study by $[P_{m1}(t) - P_{m2}(t)]/L_m$, where L_m is the (fixed) membrane length. For a given pressure gradient, since the momentum of the fluid in the boundary layer is smaller than that in the bulk solution due to the viscous effects at the wall, the changing velocity in the momentum boundary layer responds more rapidly to the pressure gradient than does that of the bulk solution. Thus flow in the boundary layer conforms more closely to the pressure-gradient variation than does flow outside the boundary layer. At the limit, where the wall enforces zero momentum, the shear is in phase with the pressure gradient.

Thus in circumstances where shear is related instantaneously to the axial pressure gradient, the maximum shear can be regarded as being proportional to the maximum pressure gradient along the membrane module, $[P_{m1}(t) - P_{m2}(t)]_{\max}/L_m$. Even in turbulent flows, where the local pressure gradient varies chaotically, the overall pressure gradient can be expected to provide a measure of the shear at the membrane surface. Therefore the maximum of the absolute pressure difference along the membrane module, $|P_{m1}(t) - P_{m2}(t)|_{\max}$, is usable as an empirical relative measure of the effect of shear on particle deposition.

In deriving $|P_{m1}(t) - P_{m2}(t)|_{\max}$ from experimental recordings, it was found that the pressure difference along the membrane module in this study was relatively small compared with the transmembrane pressure. Due to zero drift in the pressure transducers, the experimental error involved in measuring the pressure gradient could become large. Hence, it was decided that the maximum of the absolute derivative of cross-flow velocity, $|dV_{cf}(t)/dt|_{\max}$, which was determined to be linearly related to $|P_{m1}(t) - P_{m2}(t)|_{\max}$ (Bertram, 1980), could be used to evaluate the effect of shear

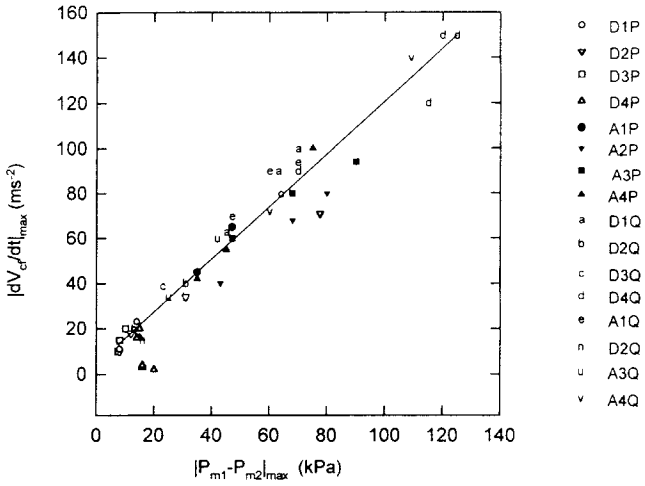

Figure 1. Maximum absolute value of velocity derivative vs. pressure gradient along the membrane tubes, showing a linear relationship between these two parameters.

Those pulsatile flows were used in the filtration experiments (Figures 2 and 4). A, D = rig configurations (Figure 4); P, Q = servo inputs for the defined waveshape of pressure and flow rate, respectively; and 1, 2, 3, 4 = waveforms (Figure 2). The line is the linear regression of all data.

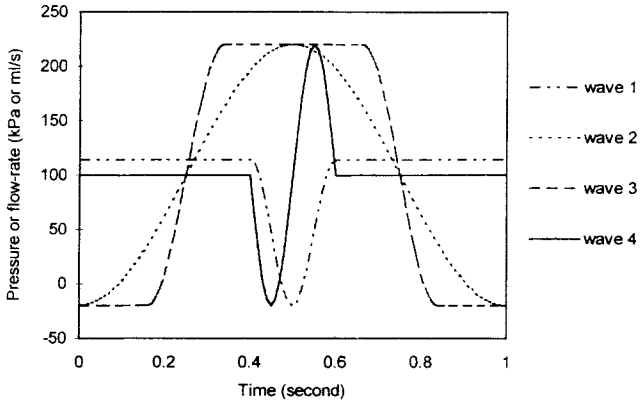

Figure 2. Designed waveforms for pressure and flow rate.

Wave 1, dash-dot; wave 2, dotted; wave 3, dashed; wave 4, solid line. All the waves had the same mean values and the same minimum; except for wave 1, all the waves had the same amplitude.

on filtration behavior. The relationship between $|dV_{cf}(t)/dt|_{max}$ and $|P_{m1}(t)-P_{m2}(t)|_{max}$ for 16 pulsatile flows is illustrated in Figure 1.

Experimental Method

Selection of idealized waveforms

To characterize the ways in which waveform shape can influence the effectiveness of a pulsatile flow, and to reduce the number of experiments, we chose a small number of distinct waveforms for transmembrane pressure and cross-flow velocity. Since the effectiveness of any given waveform shape is likely to increase with frequency, frequency was maintained constant, at 2 Hz. The mean values of transmembrane pressure and cross-flow velocity were also maintained constant, at 100 kPa and 1 m/s, respectively.

For the pressure waveform, the major concerns were the minimum value of the transmembrane pressure, P_{min}; the duration of the negative pressure; and the rate of pressure variation. Four basic waveforms were selected for the experimental tests in this study, as illustrated in Figure 2. Wave-type 1 had a long steady-pressure phase and a short, negative low-pressure pulse, akin to what is provided by collapsible-tube pulsation. For this wave, when the pressure was lower than zero, backflushing was expected to take place. The duration of the negative pressure was short compared to the period of the waveform. Wave-type 2 had an approximately sinusoidal form; it provided smooth variation of the pressure. The duration of the negative pressure was longer than in wave-type 1, and the rate of pressure change was lower than in wave 1, but the minimum pressure reached was the same. Wave-type 3 was approximately square shaped, having the same amplitude of pressure variation as wave 2, and the same minimum pressure as both waves 1 and 2, but the longest negative pressure duration. Wave-type 4 had a shortened sinusoidal disturbance, providing rates of pressure change comparable to (but slightly higher than) those in waves 1 and 3, but without the asymmetry of wave 1. These four pressure waveforms represented the smallest number that would allow independent variation of each of the features of the pulsation deemed important, so that the relative importance of these features in terms of cake reduction could be determined.

For the flow-rate wave, the concern was to provide a wide range of shear variation in terms of the parameter $|dV_{cf}(t)/dt|_{max}$ through variation of the flow-rate waveform. The important features of the waveform were the suddenness of flow-rate change, amplitude, and the shape, which all relate to the rms shear. Four waveforms of flow-rates corresponding approximately in shape to the four waveforms of pressure presented in Figure 2 were developed; however, these flow-rate waveforms necessitated quite different inputs to the servo-controlled actuator than did their pressure counterparts.

Independent variation of shear and backflushing

In order to distinguish between the two proposed mechanisms, it was intended to maintain one effect (shear or backflushing) constant while changing the magnitude of the other effect for each waveform shape. A simulation of the fluid circulation in the system was conducted to demonstrate the possibility of independent variation of the selected parameters (P_{min} and $|dV_{cf}(t)/dt|_{max}$). The computer simulation of an equivalent electrical analog circuit with only linear components is described in the Appendix. Figure 3 shows the filtration apparatus that was simulated.

The simulation results suggested that a given pressure waveform, shape, and amplitude could indeed be held constant, while the flow-rate waveform was free to vary and vice versa. This could be achieved by a combination of changes in rig configuration along with carefully devised input signals for the servo actuator.

The configuration changes explored in the simulation amounted to changing the reservoir compliance and the fluid inertance downstream of the membrane. Equivalent realiz-

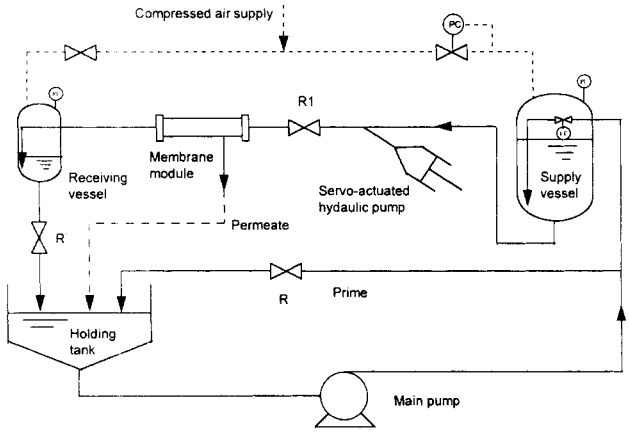

Figure 3. Filtration apparatus.

PI = pressure indicator; PC = pressure controller; LC = level controller; R, R′ = variable pressure-relief valve; R_1 = ball valve.

able variations in the configuration of the filtration apparatus shown in Figure 3 were bypassing or including the receiving vessel tank in the flow circulation, and placing the membrane module upstream or downstream of a one-meter-long flexible

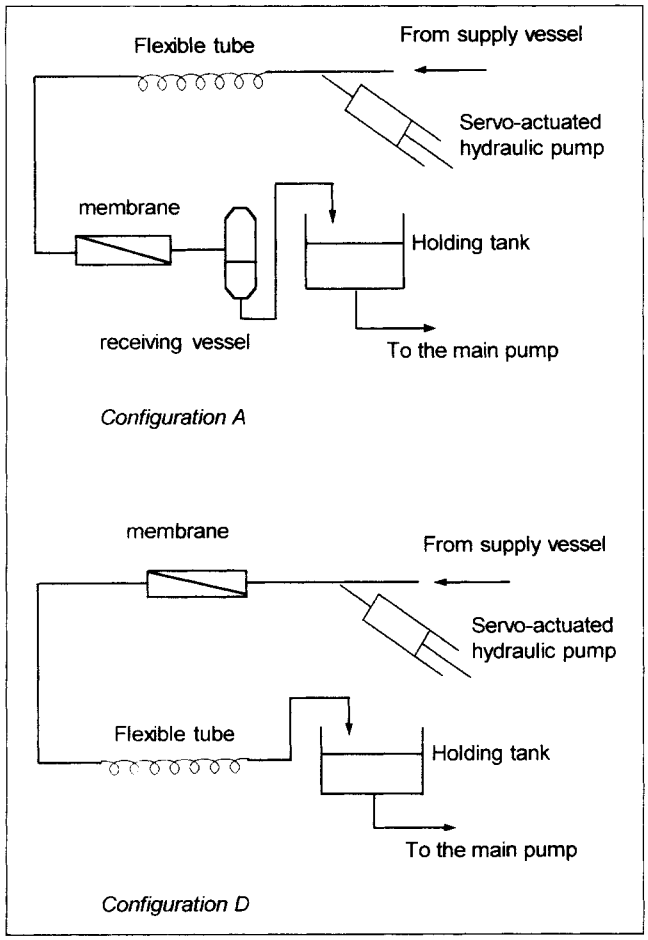

Figure 4. Selected rig configurations for the filtration tests.

The main pump and the holding tank in the flow circulation are not shown, but were the same for both configurations.

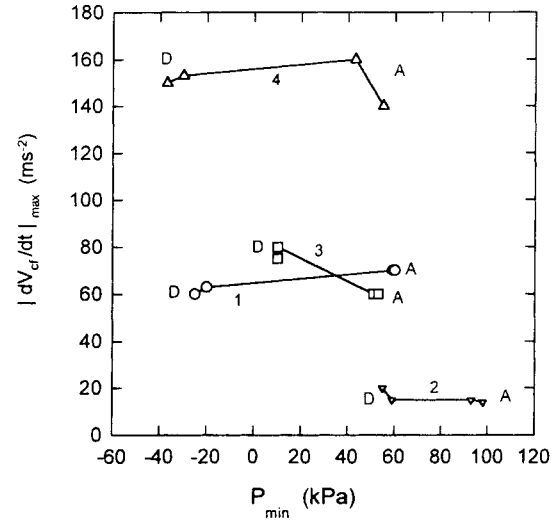

Figure 5. Rate of velocity change vs. the minimum transmembrane pressure for four waveforms and two rig configurations.

The amplitude of each flow-rate waveform was kept approximately the same (200 ± 5 mL/s) by changing the command signal for each rig configuration. The figure shows values for duplicate tests: A, D = rig configurations. The numbers indicate the waveforms in Figure 2.

connecting tube (not shown). Among these possibilities, including or omitting the receiving vessel was found experimentally (as in simulation) to provide wider parameter variations than varying the inertance downstream of the membrane module. Two configurations, A with the membrane module downstream of the flexible tube and with the downstream tank in the circulation line, and D with the membrane module upstream of the flexible tube and the downstream tank bypassed, were selected for the filtration tests. Figure 4 shows these two rig configurations. Figures 5 and 6 present

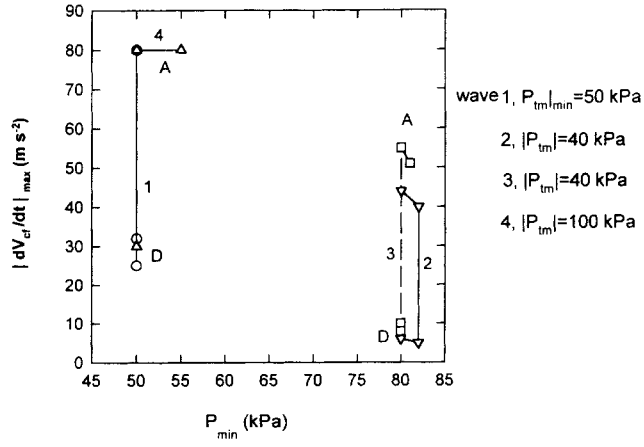

Figure 6. Rate of velocity change vs. the minimum transmembrane pressure for four waveforms and two rig configurations.

The amplitude of each pressure waveform was kept approximately the same by changing the command signal for each rig configuration. Duplicate measurements are shown: A, D = rig configurations. The numbers indicate the waveforms as in Figure 2.

experimental measurements of the variation of P_{min} and $|dV_{cf}(t)/dt|_{max}$ for various combinations of rig configuration and flow-rate and pressure waveform.

Experimental apparatus

The components in the experimental apparatus were illustrated in Figure 3. The exact rig configuration for each experiment varied as described in the previous section. The main pump fed the supply vessel through a level control valve at the inlet of the vessel. The supply vessel was pressurized with air. When required (configuration A), a closed receiving vessel was inserted downstream of the membrane module before the fluid returned to the holding tank. By manipulating the pressure in the supply tank and the resistance to flow back to the holding tank, the mean transmembrane pressure and cross-flow velocity in the membrane tubes could be adjusted independently. A ceramic membrane of 0.2-μm pore size (Ceraflo, Millipore) was used for the experiments. The membrane was in the form of a monolith, with 19 cylindrical bores of 2.5-mm and 405-mm length, cut to fit an available stainless-steel housing.

An electrohydraulic-controlled-position servo system (Moog Australia) was applied to a piston-in-cylinder as the pulsatile-flow generator. This generator was connected as a branch on the main fluid-flow recirculation conduit. In this way, flow oscillation from the hydraulic pump branch was superimposed onto the main flow. The command waveform to the piston pump for each required flowrate or pressure waveform in the membrane module was obtained by system identification and modification through experimental iterations. The waveform was synthesized digitally and converted to an electrical signal using a 12-bit digital-to-analog (d/a) converter.

The mean values and waveforms of P_{tm} and cross-flow-rate Q were monitored using voltmeters and oscilloscopes, respectively. The instantaneous pressures (P_{m1}, P_{m2}, and the pressure upstream of the hydraulic pump) were measured with wide-band pressure transducers (Kulite XTM-190). The transmembrane pressure was obtained by connecting signals from transducers at P_{m1} and P_{m2} to an analog summer to produce the output signal $P_{tm} = (P_{m1} + P_{m2})/2$. The instantaneous flowrate into the membrane module was measured with an SWF-5 square-wave electromagnetic (EM) flowmeter (Zepeda Instruments). The instantaneous permeate flux was measured using another EM flowmeter probe. The signal was fed to both the main digitizing system and a separate analog-to-digital (a $\neq$ d) board (DT2814, Data Translation) for calculation of the average permeate flux over 30 s.

The instantaneous input signal to the hydraulic pump, the pressures upstream of the hydraulic pump, up- and downstream of the membrane module (P_{m1} and P_{m2}), flowrate upstream of the membrane module (Q), and permeate flux (J), were digitized simultaneously by a 12-bit data-acquisition system (DT 2752 and DT 2769, Data Translation). The sampling rate was 500 Hz. The recordings were normally made over 2-s time periods. Thus, with a fluid oscillation frequency of 2 Hz, four complete waveforms were recorded.

Control tests

Control tests of filtration using distilled water as feed were carried out for all pulsatile flows, that is, all waveform and rig-configuration variations. The flux under steady-flow conditions was measured before and after each pulsatile-flow condition. All the flux measurements at steady and pulsatile conditions were taken for 45 min. After each 45-min measurement, the membrane module was taken out of the rig and backflushed with distilled water to measure the membrane resistance.

Filtration tests

A 0.5 g/L silica suspension was used for the microfiltration experiments. The mean particle size was 3.85 μm, with a standard deviation of 3.75 μm, as measured by a Mastersizer/E (Malvern Instruments, England).

For each pulsatile flow, filtration under steady-flow conditions was conducted both before and afterwards. As for the controls, all the filtration tests were conducted for 45 min. The membrane was backflushed after each 45-min test. The membrane resistance was estimated from the backflushing flowrate. Before each steady–pulsatile–steady test series, the membrane was chemically washed by soaking in hypochlorite solution for 30 min, then backflushed with 2 L of MilliQ water. In this way, the membrane resistance at the commencement of each test was approximately constant.

Cake resistance was calculated from the filtration flux measurement, using the resistance model

$$R_c = \frac{P_{tm}}{\mu J} - R_m, \tag{1}$$

where R_c is the cake resistance, P_{tm} is the transmembrane pressure, μ is the viscosity, J is the flux, and R_m is the membrane resistance. Note that flux J is a time-varying parameter. Thus, the value of R_c changes over time. For the purposes of determining the effect of pulsatile flow in the experiments, the cake resistances for steady and pulsatile flow were determined at 45 min. The cake-resistance reduction for pulsatile flow compared with the corresponding steady flow was calculated as

$$\zeta = \frac{R_{c,s} - R_{c,p}}{R_{c,s}}, \tag{2}$$

where $R_{c,s} = (R_{c,s1} + R_{c,s2})/2$; $R_{c,p}$, $R_{c,s1}$ and $R_{c,s2}$ are cake resistance in the pulsatile flow, and in the first and second steady flows. The reason for using cake-resistance reduction rather than flux enhancement to represent the effect of pulsatile flow is explained in the Discussion section.

Results

Control tests

Figure 7 presents the results of the control tests for four pressure waveforms with rig configuration D. Similar results were obtained for other pulsatile flows. It can be seen from Figure 7 that, as expected, fluid pulsation did not affect the flux of a pure liquid. The slight decline in flux over the total testing time was not affected by changing from steady to various pulsatile flows, or by the interruption of the test and backflushing of the membrane. The membrane resistance

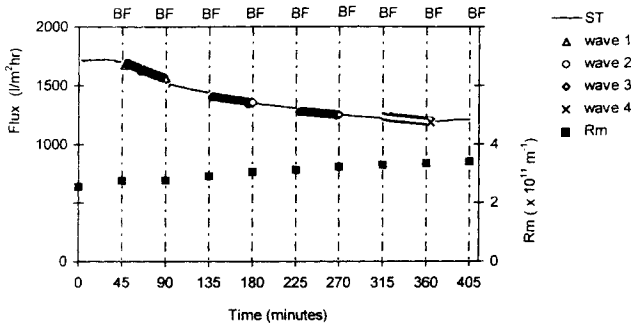

Figure 7. Flux during filtration of distilled water for pulsatile flows with four pressure waveforms and for steady flows in between the pulsatile flows, all at rig configuration D.

The membrane was backflushed and membrane resistance measured in between the changes in the cross-flow conditions. BF = backflush; ST = steady-flow.

measurement confirmed that the flux decline was indeed due to increasing membrane resistance.

Filtration tests: Shear effect

Figure 8 presents the cake-resistance reduction results as a function of the change in $|dV_{cf}/dt|_{max}$ without backflushing, that is, with positive P_{min}. The four pressure waveforms were maintained constant when the rig configuration was changed from A to D, while the flow-rate waveforms were free to change. The pulsatile flow conditions are identified with annotations indicating the rig configuration and waveform. The results in Figure 8 show that cake resistance always became less as the value of the shear-related parameter $|dV_{cf}/dt|_{max}$ increased.

Backflush effect

The effect of a periodic backflush on cake-resistance reduction was evaluated with tests in which the flow-rate waveform was maintained constant.

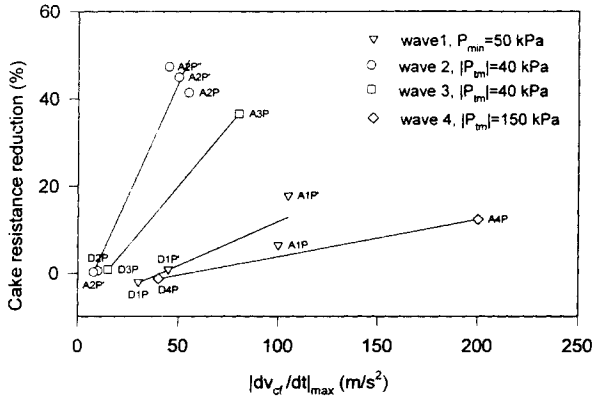

Figure 8. Influence of $|dV_{cf}/dt|_{max}$ on cake resistance reduction.

The pressure waveforms were maintained constant at configurations A and D, with the amplitudes given in the legend. Due to the nonsymmetric nature of wave 1, P_{min} was used to represent the magnitude of the wave.

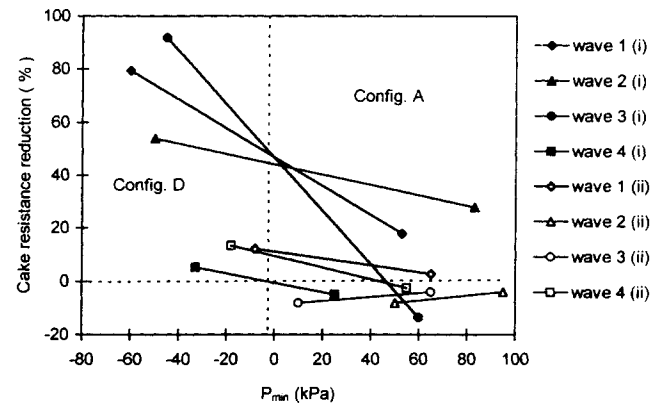

Figure 9. Cake resistance reduction vs. the minimum transmembrane pressure.

The flow-rate waveform was maintained constant for each pair of tests joined by solid lines. The data on the lefthand side of the vertical dashed line were obtained with rig configuration D, and the data on the righthand side with configuration A. The flow-rate amplitude for the first set of tests, indicated by (i), was 215 ± 15 mL/s, and the flow-rate amplitude for the second set of tests, indicated by (ii), was 320 ± 20 mL/s.

In Figure 9, the cake-resistance reductions are presented against the minimum transmembrane pressure for pairs of tests with constant flow-rate waveform. The amplitudes of flow-rate waveforms were different for tests (i) and (ii). It can be seen that, for a given flow-rate waveform, changing the minimum transmembrane pressure from positive to negative always reduced the cake resistance. Reducing the minimum in transmembrane pressure from a positive value to a smaller positive value had little effect on the cake-resistance reduction, as seen in tests with wave 2 (ii) and wave 3 (ii). Large negative values of P_{min} were more effective than small ones.

Discussion

Control tests

The increase in the membrane resistance can only be attributed to the absorption of bacteria or other species from the distilled water onto the membrane surface or in the membrane pores. Observations by Elmaleh and Naceur (1992) on the flux decline of filtration of a stored standard water (obtained by prefiltration of tap water through a 0.8-μm filter, followed by reverse osmosis and resin demineralization) provide evidence that microorganisms can develop, and might have developed, in the initially high-quality water.

The shear aspect of pulsation

Figure 8 demonstrates that, for each given pressure waveform, the cake resistance was significantly reduced at high $|dV_{cf}/dt|_{max}$ value, whereas at low $|dV_{cf}/dt|_{max}$ values no significant change in cake resistance was observed under steady-flow conditions. It is also obvious that the shape of the pressure waveform had a significant effect on the reduction of cake resistance. For instance, with waveforms 2 and 3, although the variation of $|dV_{cf}/dt|_{max}$ was smaller, much larger variations were obtained in the cake-resistance reduction than with waveforms 1 and 4.

A possible explanation can be found in the fluid dynamics of the pulsatile flows. To begin, because the flows were turbulent (Li, 1995), viscous momentum diffusion would have dominated only in the boundary layer. Particle deposition at the membrane surface takes place in the boundary layer. When the pressure gradient produces acceleration of the fluid, the thickness of the boundary layer is decreased. In this way accumulated particles, brought into the boundary layer by permeate flow through the membrane, can be partly transported back to the bulk flow by turbulence outside the boundary layer. Hence particle back-transport will be enhanced during periods of fluid acceleration. In this study, higher $| dV_{cf}/dt |_{max}$ reflects a thinner boundary layer achieved by the pulsatile flow and greater removal of the particles from the membrane surface region. Observing the velocity derivative dV_{cf}/dt of the four waveforms for rig configuration A presented in Figure 10, the duration of peak acceleration and deceleration was much longer for waveforms 2 and 3 than for waveforms 1 and 4. By offering more opportunity for momentum diffusion in the boundary layer, this longer time apparently led to greater cake-resistance reduction for waveforms 2 and 3.

The backflush effect of pulsation

Figure 9 shows that negative P_{min} values were an important factor in the reduction of cake resistance. These results suggest that instantaneous backflushing is an effective way of interrupting the particle deposition at the membrane surface. The results also show that for a given waveform with negative P_{min}, the greater the negative P_{min}, the more the cake-resistance reduction.

Comparing the four pressure waveforms for rig configuration D presented in Figure 11, it is concluded that the shape of the negative-pressure waveform also had an impact on the cake-resistance reduction. Having the shortest backflushing time, waveform 4 gave a much smaller cake-resistance reduction than did waveform 3, which has the longest backflushing time. This suggests that even with backflushing occurring transiently twice per second, the removal of particles improves with the increasing duration of backflushing. In one particular test with waveform 3, the cake-resistance reduction reached 91%. In general, the optimal duration and form of negative P_{min} would be expected to depend on the accumulation rate of particles near the membrane, the nature of the particles, and the frequency of the backflushing.

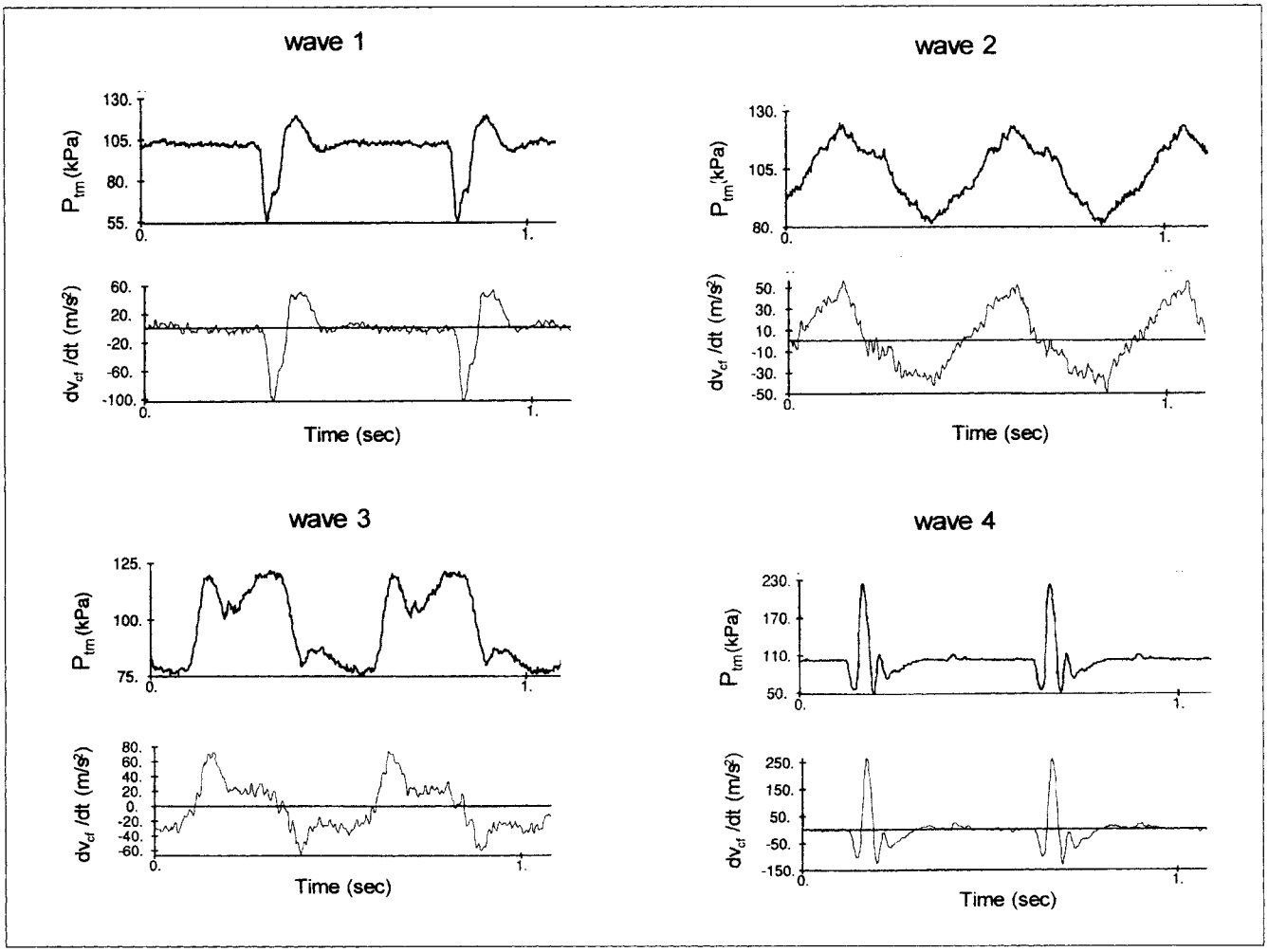

Figure 10. Waveforms of the transmembrane pressure and the derivative of cross-flow velocity in pressure-waveform-controlled tests.

Rig configuration A.

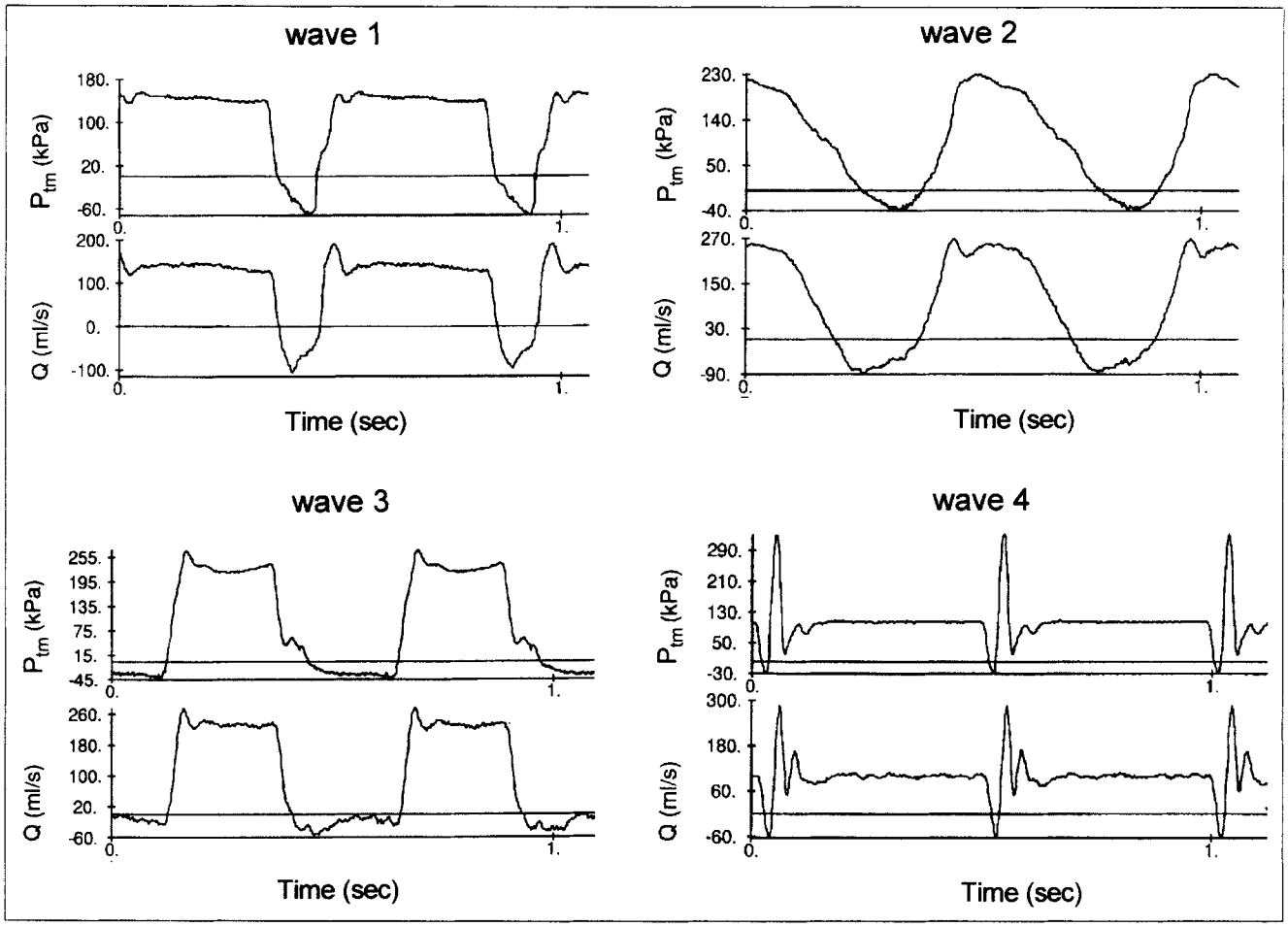

Figure 11. The waveforms of the transmembrane pressure and the cross-flow rate in flow-rate waveform-controlled tests.

Rig configuration D.

In the results of cake-resistance reduction in Figures 8 and 9 some negative values exist, although the absolute values of these negative cake reductions are relatively small (< 13.5%). This appears to mean that the cake resistances for those pulsatile flow filtrations were higher than the cake resistances during their accompanying steady-flow filtration. This phenomenon can be explained in terms of cake formation at the membrane surface. As shown in Figure 9, the cake resistances were significantly reduced when the shear-related parameter $|dV_{cf}/dt|_{max}$ exceeded a particular value for each given pressure waveform. When the shear effect is not great enough to remove all particles from the cake layer, however, it is possible that the increased and time-varying shear due to pulsatile flow caused the removal of only the bigger particles from the top of the cake. Therefore the particles in the cake layer during pulsatile flow would have been smaller than the particles in the cake layer during steady flow. Although the cake layer during pulsatile flow might be thinner, if it were composed of smaller particles, the resistance could actually be higher. The phenomenon has been called "particle classification." Changes in the particle-size distribution influencing cake resistance have already been reported (Baker et al., 1985; Fisher and Raasch, 1985; Hoogland, 1994; Mackley and Sherman, 1992) in studies of steady-flow microfiltration.

Method of assessment of pulsatile flow

In this article, cake-resistance reduction is used to measure the degree of influence of the pulsatile flow. In the past, the flux during pulsatile flow has commonly simply been compared with the flux during steady flow.

The relationship between the cake-resistance reduction and the flux can be demonstrated as follows.

Combining Eq. 2 for the cake-resistance reduction with Eq. 1 for cake resistance, and the following equation for initial water flux

$$J_w = \frac{\bar{P}_{tm}}{\mu R_m}, \tag{3}$$

the cake resistance reduction can be expressed as

$$\zeta = \frac{\dfrac{J_w}{J_s} - \dfrac{J_w}{J_p}}{\dfrac{J_w}{J_s} - 1}. \tag{4}$$

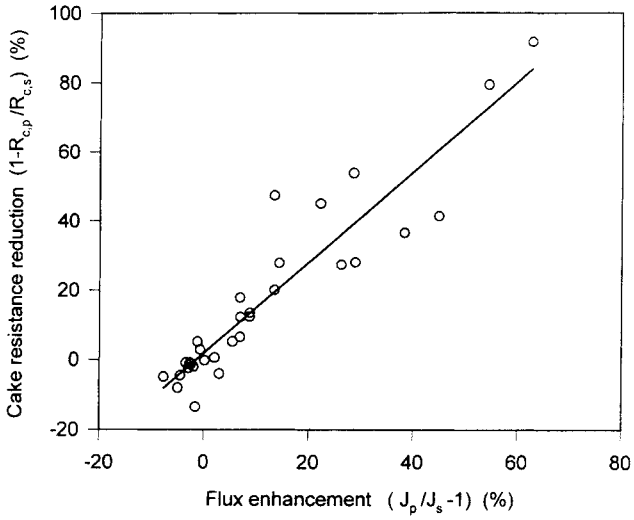

Figure 12. Comparison of cake resistance reduction and flux enhancement for the filtration.

It includes all the data from the experiments in Figures 8 and 9.

This equation relates the cake-resistance reduction to J_s and J_p, the fluxes for steady flow and pulsatile flow, and J_w, the maximum flux the membrane can achieve under the given mean values of P_{tm} and V_{cf}.

When $J_s = J_w$, the flux cannot be improved by any means. When $J_p = J_w$, $\zeta = 1$, and there is no cake resistance during filtration. When $J_p = J_s$, $\zeta = 0$, and the pulsatile flow has no effect on the cake resistance. Flux enhancement is of course defined as $J_p/J_s - 1$. Figure 12 shows that a linear relation existed between flux enhancement and cake-resistance reduction for all the filtration tests conducted in this study.

The advantage of using cake-resistance reduction instead of flux enhancement is that it gives a measure not only of how much cake resistance was reduced by pulsatile flow, but also of the extent of the flux enhancement compared to the maximum flux achievable in the absence of slurry particles, J_w. In two of the tests the cake-resistance reductions were 91% and 79%, which we immediately know is close to the maximum achievable. The same cannot be said for flux enhancements, which have no absolute reference point. Thus, while some investigators have reported that flux was increased severalfold by the application of pulsatile flow (Colman and Mitchell, 1990), it is difficult to evaluate how well these pulsatile systems were performing in comparison to the maximum achievable flux. As Figure 12 shows, however, flux enhancement and cake-resistance reduction are different measures of system performance; one is not derivable from the other. The relationship between them is likely also to be system specific. This implies that both have their place in evaluating system performance, and particularly in comparing different systems, and it would probably be best to enumerate both factors.

Conclusions

This investigation of the effect of pulsatile flow on particle deposition has demonstrated that it is possible, by a suitable choice of pulsatile conditions, essentially to eliminate the formation of cake during microfiltration.

The filtration tests with 0.5 g/L silica suspensions with variation of shear while maintaining pressure waveforms constant demonstrated that without backflushing, cake-resistance reduction occurred for all four types of flow-rate waveform when sufficient values of the shear-related parameter $|dV_{cf}/dt|_{max}$ were reached. With lower $|dV_{cf}/dt|_{max}$ values, the shear effect on cake resistance was either insignificant or even negative. It was observed that the effect of shear on cake resistance differed with the shape of the pressure wave. For the pulsations with more gradual pressure variation, the cake-resistance reductions were greater, although their $|dV_{cf}/dt|_{max}$ values were lower compared with the waves involving more abrupt pressure changes over a shorter time.

The filtration tests with and without backflushing while maintaining the flow-rate waveform constant demonstrated that, given similar levels of shear, the cake resistance was reduced when the minimum in transmembrane pressure became negative. For a given waveform, the cake resistance was reduced more with more negative P_{min} values. In two tests, the cake resistance was almost completely eliminated by including backflushing in the pulsatile flow.

Comparing the cake-resistance reductions attributable to shear and to backflushing, greater reductions were obtained through backflushing. In all tests, it was demonstrated that with the quasi-square pressure waveform the backflushing and fluid deceleration times were both longer than for the other waveforms, and cake resistance reduction was high. Pulsatile flows with briefly interrupted flowrate or pressure waveforms were not so effective in reducing cake resistance.

Thus not all pulsatile flows are equally beneficial to the filtration process. When there is no backflushing, shear alone will only improve flux performance under certain conditions. Therefore in the application of pulsatile techniques, it is advisable to identify which pulsation factor will dominate.

For applications affected by shear alone, consideration should be given to the following aspects:

1. If the materials in the suspension are shear-sensitive, temporary high shear may harm the feed.
2. The effect of shear is most beneficial for suspensions with a narrow particle-size distribution. For suspensions with a large particle-size distribution, pulsation may cause particle classification and lead to increased cake resistance and decreased flux.
3. Much of the beneficial effect of shear is associated with higher-amplitude flow-rate variation, which implies higher energy costs during operation.

For applications of pulsatile flow where backflushing is appropriate, enhanced flux is almost guaranteed. The advantages of using backflushing instead of shear to reduce cake formation are as follows:

1. The effect of backflushing does not require specific mean operating conditions. The process can be operated at lower mean flowrates and transmembrane pressures, thereby reducing operating costs.
2. Backflushing is independent of the particle-size distribution of the suspension, and should therefore be applicable to the filtrations of difficult suspensions or solutions including biomaterials. In fractionation applications, which require the maintenance of a strict sieving factor at the membrane sur-

face, backflushing should prevent particle deposition, thereby maintaining the size separation.

Generally, pulsatile flow can be applied most easily to the tubular and hollow-fiber membrane configurations. For other membrane module configurations, more tests still need to be conducted. Ceramic and other membranes with a rigid structure are likely to benefit most from the application of a pulsatile flow. For nonrigid membranes the pressure changes generated by the pulsation are partially dissipated by elastic motion of the entire membrane and substrate. While such motion itself may confer temporary advantages, it is likely to lead to reduced membrane life.

Notation

i_1, i_m, i_s = currents (ampere) simulating flowrate (m^3/s) upstream of the hydraulic pump, in the membrane module, and in the hydraulic-pump branch
r = tube radius, m
t = time, s
v_2, v_{cs} = voltage (V), simulating pressures across the capacitor C_2, and C_s
V_{cf} = cross-flow velocity, $m \cdot s^{-1}$
ν = momentum diffusivity, $m^2 \cdot s^{-1}$
ω = radian frequency, s^{-1}

Literature Cited

Baker, R. J., A. G. Fane, C. J. D. Fell, and B. H. Yoo, "Factors Affecting Flux in Crossflow," *Desalination*, **53**, 81 (1985).

Batchelor, G. K., *An Introduction to Fluid Dynamics*, Cambridge Univ. Press, Cambridge (1970).

Bertram, C. D., "Energy Dissipation and Pulse Wave Attenuation in the Canine Carotid Artery," *J. Biomech.*, **13**, 1061 (1980).

Bertram, C. D., M. R. Hoogland, H. Li, R. A. Odell, and A. G. Fane, "Flux Enhancement in Crossflow Microfiltration Using a Collapsible-Tube Pulsation Generator," *J. Memb. Sci.*, **84**, 279 (1993).

Colman, D. A., and W. S. Mitchell, "Enhanced Mass Transfer for Membrane Processes," *Inst. Chem. Eng. Symp.*, **118**, 119 (1990).

Davis, R. H., and S. A. Birdshell, "Hydrodynamic Model and Experiments for Crossflow Microfiltration," *Chem. Eng. Commun.*, **49**, 217 (1987).

Ding, L., J. M. Laurent, and M. Y. Jaffrin, "Dynamic Filtration of Blood: A New Concept for Enhancing Plasma Filtration," *Int. J. Artif. Organs*, **14**, 365 (1991).

Ding, L. H., M. Y. Jaffrin, and M. Defossez, "Concentration Polarization Formation in Ultrafiltration of Blood and Plasma," *J. Memb. Sci.*, **84**, 293 (1993).

Elmaleh, S., and W. Naceur, "Transport of Water Through an Inorganic Composite Membrane," *J. Memb. Sci.*, **66**, 227 (1992).

Fane, A. G., "Ultrafiltration: Factors Influencing Flux and Rejection," *Progress in Filtration and Separation*, Vol. 4, R. J. Wakeman, ed., Elsevier, New York, p. 101 (1986).

Fisher, E., and J. Raasch, "Cross-Flow Filtration," *Ger. Chem. Eng.*, **8**, 211 (1985).

Gupta, B. B., P. Blanpain, and M. Y. Jaffrin, "Permeate Flux Enhancement by Pressure and Flow Pulsations in Microfiltration with Mineral Membranes," *J. Memb. Sci.*, **70**, 256 (1992).

Gupta, B. B., L. H. Ding, and M. Y. Jaffrin, "High Efficiency Small Membrane Area Plasmapheresis Using Pulsatile Blood Flow," *Progress in Artificial Organs*, Y. Nosé, C. Kjellstrand, and P. Ivanvich, eds., ISAO Press, Cleveland, p. 891 (1986).

Hoogland, M. R., "The Crossflow Microfiltration of Mineral Slurries," PhD Thesis, The Univ. of New South Wales, Sydney, Australia (1994).

Ilias, S., and R. Govind, "Potential Applications of Pulsed Flow for Minimizing Concentration Polarization in Ultrafiltration," *Sep. Sci. Technol.*, **25**, 13 (1990).

Jaffrin, M. Y., "Innovative Processes for Membrane Plasma Separation," *J. Memb. Sci.*, **44**, 115 (1989).

Jaffrin, M. Y., R. Ben Amar, and B. B. Gupta, "Membrane Fouling Control in Cross Flow Filtration of Wine with Mineral Membranes," *Proc. Int. Tech. Conf. on Membrane Separation Processes*, Brighton, UK (1989).

Jaffrin, M. Y., L. H. Ding, and B. B. Gupta, "Rationale of Filtration Enhancement in Membrane Plasmapheresis by Pulsatile Blood Flow," *Life Support Syst.*, **5**, 267 (1987).

Jaffrin, M. Y., L. H. Ding, and J. M. Laurent, "Kinetics of Concentration-Polarization Formation in Cross-Flow Filtration of Plasma from Blood: Experimental Results," *J. Memb. Sci.*, **72**, 267 (1992).

Jaffrin, M. Y., B. B. Gupta, and P. Paullier, "Energy Saving Pulsatile Mode Cross-Flow Filtration," *J. Memb. Sci.*, **86**, 281 (1994).

Kennedy, T. J., R. L. Merson, and B. J. McCoy, "Improving Permeation Flux by Pulsed Reverse Osmosis," *Chem. Eng. Sci.*, **29**, 1927 (1974).

Li, H., "Mechanism Studies for Crossflow Microfiltration with Pulsatile Flow," PhD Thesis, The Univ. of New South Wales, Sydney, Australia (1995).

Mackley, M. R., and N. E. Sherman, "Cake Filtration Mechanisms in Steady and Unsteady Flows," *Proc. Eng. Memb. Process*, Bavaria, Germany (1992).

McDonald, D. A., *Blood Flow in Arteries*, Arnold, London (1974).

Rodgers, V. G. J., and R. E. Sparks, "Reduction of Membrane Fouling in the Ultrafiltration of Binary Protein Mixtures," *AIChE J.*, **37**, 1517 (1991).

Rodgers, V. G. J., and R. E. Sparks, "Effect of Transmembrane Pressure Pulsing on Concentration Polarization," *J. Memb. Sci.*, **68**, 149 (1992).

Spiazzi, E., J. Lenoir, and A. Grangeon, "A New Generator of Unsteady-State Flow Regime in Tubular Membranes as Anti-Fouling Technique: A Hydrodynamic Approach," *J. Memb. Sci.*, **80**, 49 (1993).

Wenten, I. G., D. M. Koenhen, H. D. W. Roesink, A. Rasmussen, and G. Jonsson, "The Backshock Process—A Novel Backflush Technique in Microfiltration," *Proc. Eng. Memb. Process II, Environmental Applications*, Il Ciocco,, Tuscany, Italy (1994).

Winzeler, H. B., and G. Belfort, "Enhanced Performance for Pressure-Driven Membrane Processes: The Argument for Fluid Instabilities," *J. Memb. Sci.*, **80**, 35 (1993).

Zydney, A. L., and C. K. Colton, "A Concentration Polarization Model for the Filtrate Flux in Crossflow Microfiltration of Particulate Suspensions," *Chem. Eng. Commun.*, **47**, 1 (1986).

Appendix: Simulation of an Electric Analog of the Pulsatile Flow Circuit

In the electric-circuit simulation, voltage and current behave like pressure and flow rate, respectively, in the fluid circuit. A network of resistors, capacitors, and inductors can be devised to represent the viscous resistances, compliances, and inertances in the pulsatile flow. The equivalence between the hydrodynamic parameters and the electric parameters is given in Table A1. Well-known mathematical expressions and the numerical simulation of the analog electrical circuit itself through digital programming make a convenient method for estimating the behavior of the pulsatile fluid sys-

Table A1. Equivalent Electric Circuit and Fluid Dynamic Parameters

Electric Variables		Hydraulic Variables	
Name and Unit	Relations	Name and Unit	Relations
Current (A)	i	Flow rate (m^3/s)	Q
Voltage (V)	v	Pressure (kPa)	P
Resistance (Ω)	$R = v/i$	Resistance ($kPa \cdot s/m^3$)	$R = P/Q$
Capacitance (F)	$C = i/(dv/dt)$	Compliance (m^3/kPa)	$C = U_{air}/P$
Inductance (H)	$L = v(di/dt)$	Inertance ($kPa \cdot s^2/m^3$)	$L = \rho l/S$

U_{air} = volume of air in a vessel; ρ = fluid density; l = tube length; S = tube cross-section area.

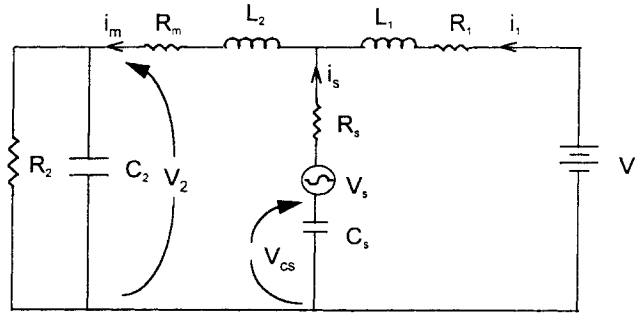

Figure A1. Electric analog simulation of the fluid circulation in the filtration rig with the flexible tube upstream of the membrane module.

tem. Such an electric analog can be used to compute the effects of any changes in system parameters on system performance.

Since the fluid circulation was mostly in rigid tubes, and the feed was an aqueous suspension, the velocity of wave transmission in the fluid-flow system was high enough that the distributed properties of the system could be neglected. Therefore the use of a lumped-parameter model in this simulation was justified.

Figure A1 shows the electric circuit that is equivalent to the filtration circuit. The flow in the hydraulic-pump branch was simulated with an alternating voltage source V_s, a resistor R_s, and a capacitor C_s in series to prevent dc in this line. The constant pressure in the supply vessel was represented by a constant voltage source V; given that V was constant, no representation of the compliance in the upstream tank was needed in the model. The valve upstream of the hydraulic pump was represented by a resistor R_1; the membrane module was represented by a resistor R_m; and the closed receiving vessel together with the pressure-relief valve at the outlet were represented by the capacitor C_2 in parallel with the resistor R_2. The inertance of the fluid in the conduit from the upstream to the downstream tank was divided into two sections, one upstream of the hydraulic pump, L_1, and one downstream, L_2.

The dynamic equations for the circuit were obtained from the Kirchhoff equations for electrical circuits:

For the V–V_s loop:

$$V - R_1 i_1 - L_1(di_1/dt) + R_s i_s - V_s - v_{cs} = 0,$$

For the V_s–V_2 loop:

$$v_{cs} + V_s - R_s i_s - R_m i_m - L_2(di_m/dt) - v_2 = 0.$$

Summing currents at the junctions,

$$i_m = v_2/R_2 + C_2(dv_2/dt)$$

and

$$i_m = i_1 + i_s.$$

The system is fourth order, and with an additional equation $i_s = C_s(dv_{cs}/dt)$, the preceding equations can be reorganized in the standard simultaneous first-order differential form:

$$L_2\frac{di_m}{dt} = v_2 + R_s i_1 - v_2 - (R_s + R_m)i_m + v_{cs} \quad \text{(A1)}$$

$$L_1\frac{di_1}{dt} = V - V_s(t) - (R_s + R_1)i_1 + R_s i_m - v_{cs} \quad \text{(A2)}$$

$$C_2\frac{dv_2}{dt} = i_m - \frac{v_2}{R_2} \quad \text{(A3)}$$

$$C_s\frac{dv_{cs}}{dt} = -i_1 + i_m. \quad \text{(A4)}$$

While v_{cs} is not a variable with an experimentally measurable counterpart, this set of dependent variables does result in a particularly simple form of the equations.

In the preceding equations, R_1, R_2, R_m, C_2, C_s, L_1, L_2, and V are constants. R_m was estimated from the pressure drop along the membrane module under steady-flow conditions,

$$R_m = (P_{m1} - P_{m2})/Q,$$

R_2 was estimated as P_2/Q, where P_2 was the pressure in the receiving tank, and was estimated for transmembrane pressure P_{tm} under steady flow. The capacitance C_2 of the receiving tank was estimated as U_{air}/P_2, where U_{air} was the trapped air volume. L_1 and L_2 were estimated as

$$L_n = \rho l_n/S_n,$$

where $n = 1$, 2, and l_n and S_n were the length and cross-sectional areas of the flow channel. The estimation of R_S and C_S was more arbitrary, but was based loosely on recognition of the finite impedance the hydraulic system presented. The simulated P_{tm} and V_{cf} signals were compared with the recordings acquired experimentally. Several iterations were needed to obtain realistic estimations of constant variables.

The ordinary differential equations (Eqs. A1–A4) were solved numerically using second- and third-order Runge-Kutta formulas from the MATLAB ode23 function package. The transmembrane pressure P_{tm} and the velocity derivative dV_{cf}/dt were evaluated from the solutions of the equations. Finally, $P_{\min}$ and $|dV_{cf}/dt|_{\max}$ were obtained.

Change in the rig configuration was simulated by changing components in the simulation circuit. Four variations were simulated. Configuration A is shown in Figure A1. In configuration B (not shown), interchanging the positions of R_m and L_2 represented moving the flexible tube from upstream to downstream of the membrane module. Configurations A and B had the same differential equations for the selected variables. With the same input signal, the flowrate (i_m in the circuit) was the same. Therefore the velocity-derivative waveform remained the same. However, the transmembrane pressure changed because P_{tm} in circuit A took the form

$$P_{tm} = v_2 + \frac{1}{2}R_m i_m, \quad \text{(A5)}$$

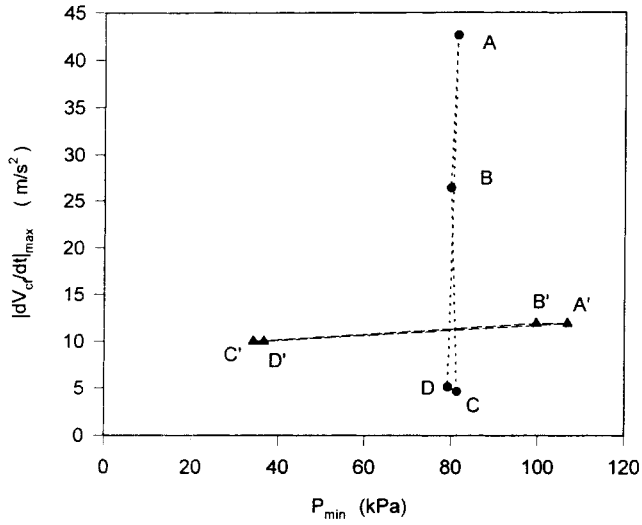

Figure A2. Simulation of independent variation of P_{min} and $|dV_{cf}/dt|_{max}$ by changing the rig configuration and the amplitude of the input signal.

A, B, C, D (connected with dotted lines) simulate the possible variations of $|dV_{cf}/dt|_{max}$ with changes in rig configuration while the pressure waveform was constant (mean P_{tm} 100 kPa, and peak-to-peak amplitude 40 kPa). A', B', C', and D' (connected with dash lines) simulate the possible variations of P_{min} with changes in rig configuration while the flow-rate waveform was constant (mean 100 mL/s, peak-to-peak amplitude 170 mL/s).

while in circuit B,

$$P_{tm} = \upsilon_{cs} + V_s + R_s(i_m - i_1) + \frac{1}{2}R_m i_m. \qquad \text{(A6)}$$

Circuits C and D (not shown) represented the situations in which the receiving tank was bypassed and the flexible tube was placed upstream and downstream of the membrane module, respectively. These circuits corresponded to circuits A and B, but with the omission of C_2.

The differential equations for circuits C and D are

$$L_2\frac{di_m}{dt} = \upsilon_{cs} + V_s(t) - (R_2 + R_m)i_m - R_s(i_m - i_1) \qquad \text{(A7)}$$

Table A2. Values of the Constant Variables in the Circuit Simulation for a Sine Waveform

Variable	Value	Variable	Value
R_1	0.3×10^6 (kPa·s·m^{-3})	L_1	5,000 (kPa·s^2·m^{-3})
R_2	1.0×10^6 (kPa·s·m^{-3})	L_2	9,750 (kPa·s^2·m^{-3})
R_m	0.2×10^6 (kPa·s·m^{-3})	C_2	8.0×10^{-5} (kPa^{-1}·m^3)
R_s	5.0×10^6 (kPa·s·m^{-3})	C_s	0.8×10^{-5} (kPa^{-1}·m^3)

$$L_1\frac{di_1}{dt} = V - V_s(t) - (R_s + R_1)i_1 + R_s i_m - \upsilon_{cs} \qquad \text{(A8)}$$

$$C_s\frac{d\upsilon_{cs}}{dt} = i_m - i_1. \qquad \text{(A9)}$$

The velocity derivative of both circuits C and D was obtained by differentiating i_m. The transmembrane pressure in circuit C was

$$P_{tm} = \upsilon_{cs} + V_s + R_s(i_m - i_1) + \frac{1}{2}R_m i_m, \qquad \text{(A10)}$$

while that in circuit D was

$$P_{tm} = \left(R_2 + \frac{1}{2}R_m\right)i_m. \qquad \text{(A11)}$$

Using the simulation, Figure A2 demonstrates how the changes in the rig configurations were used to manipulate the parameters of interest. In this simulation, $V_s(t)$ was a sine wave,

$$V_s(t) = V_{s0}\sin(2\pi ft)$$

where V_{s0} is the amplitude, and f (= 2 Hz) is the frequency of the input signal. The estimated values of the constant variables are given in Table A2.

The simulations presented in Figure A2 demonstrate that $|dV_{cf}/dt|_{max}$ could be held constant while P_{min} was varied; and that P_{min} could be maintained relatively constant while $|dV_{cf}/dt|_{max}$ was varied. The simulation suggested that switching from circuit A to circuit C would achieve the greatest variation in the two parameters.

Manuscript received Jan. 2, 1998, and revision received June 12, 1998.